JOURNAL OF GUIDANCE, CONTROL, AND DYNAMICS
Vol. 26, No. 3, May–June 2003

Multi-Input/Multi-Output Sliding Mode Control for a Tailless Fighter Aircraft

S. R. Wells* and R. A. Hess†
University of California, Davis, Davis, California 95616-5294

A frequency-domain procedure for the design of sliding mode controllers for multi-input/multi-output systems is presented. The methodology accommodates the effects of parasitic dynamics, such as those introduced by unmodeled actuators through the introduction of multiple asymptotic observers and model reference hedging. The design procedure includes a frequency-domain approach to specify the sliding manifold, the observer eigenvalues, and the hedge model. The procedure is applied to the development of a flight-control system for a linear model of the Innovative Control Effector fighter aircraft. The stability and performance robustness of the resulting design is demonstrated through the introduction of significant degradation in the control effector actuators and variation in vehicle dynamics.

Introduction

A RECONFIGURABLE control system is one that is able to compensate for sudden, potentially large, unknown failure events in real time using online adaptive control laws and/or adaptive redistribution of control effort. The objective of reconfiguration is system stability while retaining some level of required performance and handling qualities. As a research area, reconfigurable flight control has seen rapid growth in the past decade. The motivation for developing reconfigurable flight controls is clear. Failures during flight are inevitable, especially in combat aircraft. If the flight-control system is capable of stabilizing the aircraft and providing acceptable handling qualities (if the aircraft is piloted), it may be possible to save the airframe and save lives. Many reconfigurable algorithms that have been discussed in the literature involve, to some degree, 1) failure detection, 2) system identification, and 3) flight-control law reconfiguration.[1–7] The time necessary to complete these operations can be critical, especially if the airframe in question is open-loop unstable. Even direct adaptive methods like dynamic inversion with neural nets to remove inversion error[8–12] require some convergence time for adaptation. The method of sliding mode control (SMC) offers a characteristic that makes it very attractive for a reconfigurable application. The variable structure nature of the SMC controller allows it to adapt to very large parameter variations instantaneously. In fact, an SMC controller is invariant to so-called matched uncertainty. Plant uncertainties are defined as matched when they lie in the image of the plant input matrix, that is, the uncertainties affect the plant dynamics only through the plant input channels. Thus, if the system is invariant in the presence of uncertainties such as those arising from airframe damage, there exists no need to perform failure detection, system identification, or online control law redesign. Indeed, it was this potential simplicity and instantaneous adaptation time that motivated the research to be described.

The most significant shortcoming with SMC designs in control applications is their inability to accommodate unmodeled parasitic dynamics. In flight-control applications, these dynamics are typically those of the actuators driving the control effectors. One method that is known to alleviate this problem is the use of asymptotic observers.[13] A previous work by the authors demonstrates an observer-based SMC for a single-input/single-output flight-control application and introduces a frequency-domain approach for designing the sliding manifold.[14] This approach has been extended to a multi-input/multi-output (MIMO) observer-based SMC controller for an aircraft with stable unaugmented dynamics.[15] In the current work, the unstable highly coupled vehicle dynamics of the tailless Innovative Control Effector (ICE) fighter aircraft are addressed, and a frequency domain procedure for the important selection of observer eigenvalues is presented. In addition, a method of observer loop shaping that is equivalent to model reference hedging is introduced.

Received 9 April 2002; revision received 10 January 2003; accepted for publication 20 January 2003.

*Graduate Student, Department of Mechanical and Aeronautical Engineering; currently, Assistant Professor, Department of Aeronautics, U.S. Air Force Academy, CO 80840. Member AIAA.

†Professor and Vice Chairman, Department of Mechanical and Aeronautical Engineering. Associate Fellow AIAA.

MIMO Sliding Mode Control

Overview of SMC

There are several excellent survey articles regarding SMC theory and applications.[13,16–20] Hence, only a brief, simplified overview is given here, with emphasis on implementation and design issues. The key properties of a sliding mode controller are well known and are reviewed here without proof[21]:

1) While on the sliding mode, the system dynamics are invariant to matched uncertainty.

2) The hypersurface that describes $\sigma = 0$ defines the transient response of the system during the sliding mode.

3) While on the sliding mode, the trajectory dynamics are of a lower order than the original model.

Consider the uncertain system with m inputs and n states given by

$$\dot{x}(t) = \boldsymbol{A}(x,t) + \boldsymbol{B}(x,t)u(t) + f(t,x,u) \tag{1}$$

where f represents the parameter uncertainties present in the system and is assumed to be unknown, but bounded by some known function of time, system state, and control vectors. In simple terms, the objective of SMC is to define 1) m sliding surfaces or manifolds, represented in vector for as $\sigma(x) = 0$, and 2) a variable structure control given by

$$u(x,t) = \rho\,\mathrm{sgn}(\sigma) \tag{2}$$

such that the system is driven to the sliding surface $\sigma = 0$ in finite time and remains on this surface for all subsequent time. When $\sigma = 0$, a sliding mode is said to have been obtained. Equation (2) is said to describe variable structure control because the control structure is dependent on the sign of the function σ. This problem statement implies a two-step design process. First, the sliding manifold(s) must be designed. This can be accomplished by a

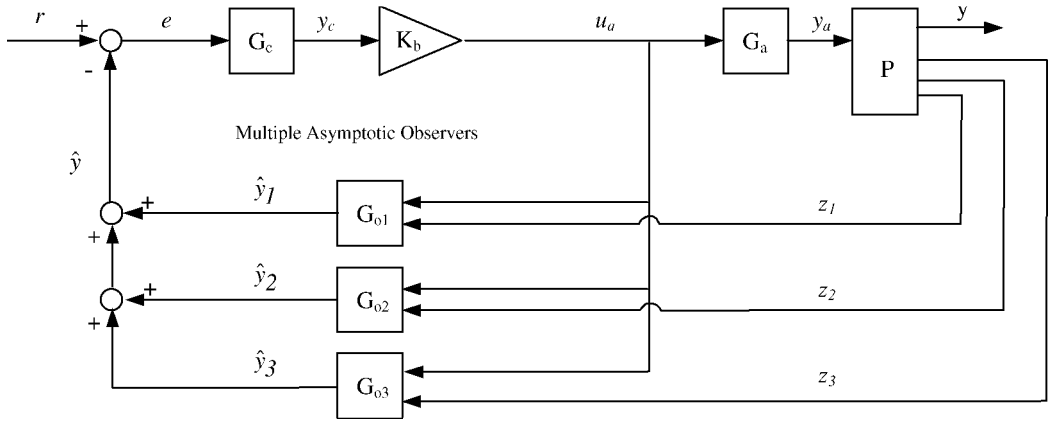

Fig. 1 Multiple observer-based SMC system.

wide variety of approaches ranging from arbitrarily selecting desired error dynamics to a linear quadratic regulator-like design approach utilizing the state equations in the so-called regular form.[21] A method that combines a square system feedback linearization approach[18,22–25] with traditional frequency domain loop shaping is used in this work. The second step in the design process is to select ρ such that the reaching condition is met. This can be done analytically using a Lyapunov stability criteria or simply by use of computational simulation.

SMC Implementation Issues

The control law in Eq. (2) is undefined while $\sigma = 0$; therefore, the control effort required to maintain the ideal sliding mode is discontinuous, with an infinite frequency switching. This control signal is unacceptable for actual mechanical systems, and a continuous implementation of an SMC is almost always sought. One of the most common approaches to obtain a continuous control signal is the inclusion of a so-called boundary layer near the sliding surface. This can be done by replacing the signum function in Eq. (2) with a finite slope line with limits at ± 1, as shown in Eq. (3):

$$u(x, t) = \rho \,\mathrm{sat}(\sigma/\varepsilon) \tag{3}$$

Another implementation issue with SMC controllers is the problem of unmodeled parasitic dynamics. The interaction of these parasitic dynamics with the SMC controller (even when a boundary layer is used) results in chatter and very often causes system instability. A simple solution to the actuator problem might be the inclusion of the actuator in the SMC design. Unfortunately, this is difficult to implement in practice because of the increased order of the sliding manifold associated with the additional dynamics. In general, the order of the manifold will increase by the same order as the modeled actuator dynamics. This means that, for a second-order actuator, at least two derivatives of the output signal are required. For a real system with measurement noise, these additional derivatives make this approach unattractive. There are several other approaches that have been proposed.[13] One that is both effective and intuitively appealing is the use of an asymptotic observer.

Observer-Based SMC

Asymptotic observers construct a "high-frequency bypass loop," essentially hiding the unmodeled parasitic dynamics from the SMC controller.[13] Selection of the observer eigenvalues is a crucial part of the observer-based SMC design. If the observer eigenvalues (and, hence, gains) are too large, chatter and instability result. In addition, sensor noise becomes a problem. If the observer eigenvalues (and gains) are too small, robustness to system parameter variation is lost. A method is sought to select the observer gains. Because a MIMO square system architecture effectively decouples the control variables, it can be shown that multiple observers (one for each control variable and each with its own eigenvalues) are desired for reducing the interaction of each sliding mode control action with the parasitic dynamics. Such an architecture is shown in Fig. 1 and is directed toward the specific flight-control application to be discussed in the design example. Consider the following system definitions corresponding to Fig. 1:

$$x \in \Re^n, \qquad x_a \in \Re^{n_a}, \qquad x_c \in \Re^{n_c}, \qquad x_r \in \Re^{n_r}$$

$$\hat{x}_{o1} \in \Re^{n_{o1}}, \qquad \hat{x}_{o2} \in \Re^{n_{o2}}, \qquad \hat{x}_{03} \in \Re^{n_{o3}}$$

$$y \in \Re^{m_y}, \qquad y_a \in \Re^{m}, \qquad y_c \in \Re^{m_y}, \qquad y_r \in \Re^{m_y}$$

$$\hat{y}_1 \in \Re^{m_y}, \qquad \hat{y}_2 \in \Re^{m_y}, \qquad \hat{y}_3 \in \Re^{m_y}$$

$$z_1 \in \Re^{m_{z1}}, \qquad z_2 \in \Re^{m_{z2}}, \qquad z_3 \in \Re^{m_{z3}}, \qquad \hat{y} \in \Re^{m_y} \tag{4}$$

Linear plant:

$$\dot{x} = \boldsymbol{A}x + \boldsymbol{B}y_a, \qquad y = \boldsymbol{C}_y x + \boldsymbol{D}_y y_a, \qquad z_1 = \boldsymbol{C}_{z1} x + \boldsymbol{D}_{z1} y_a$$

$$z_2 = \boldsymbol{C}_{z2} x + \boldsymbol{D}_{z2} y_a, \qquad z_3 = \boldsymbol{C}_{z3} x + \boldsymbol{D}_{z3} y_a$$

Actuators:

$$\dot{x}_a = \boldsymbol{A}_a x_a + \boldsymbol{B}_a \boldsymbol{K}_b y_c, \qquad y_a = \boldsymbol{C}_a x_a + \boldsymbol{D}_a \boldsymbol{K}_b y_c$$

Reference model:

$$\dot{x}_r = \boldsymbol{A}_r x_r + \boldsymbol{B}_r r_p, \qquad y_r = \boldsymbol{C}_r x_r + \boldsymbol{D}_r r_p$$

Observer 1:

$$\dot{\hat{x}}_1 = (\boldsymbol{A}_{o1} - \boldsymbol{G}_1 \boldsymbol{C}_{z1})\hat{x}_1 + \boldsymbol{B}_{o1} \boldsymbol{K}_b y_c + \boldsymbol{G}_1 z_1, \qquad \hat{y}_1 = \boldsymbol{C}_{o1} \hat{x}_1$$

where $\boldsymbol{C}_{o1} \in \Re^{m_y \times n}$ with zeros in the rows corresponding to states not output by observer 1. $\boldsymbol{G}_1 =$ observer gains.

Observer 2:

$$\dot{\hat{x}}_2 = (\boldsymbol{A}_{o2} - \boldsymbol{G}_2 \boldsymbol{C}_{z2})\hat{x}_2 + \boldsymbol{B}_{o2} \boldsymbol{K}_b y_c + \boldsymbol{G}_2 z_2, \qquad \hat{y}_2 = \boldsymbol{C}_{o2} \hat{x}_2$$

where $\boldsymbol{C}_{o2} \in \Re^{m_y \times n}$ with zeros in the rows corresponding to states not output by observer 2. $\boldsymbol{G}_2 =$ observer gains.

Observer 3:

$$\dot{\hat{x}}_3 = (\boldsymbol{A}_{o3} - \boldsymbol{G}_3 \boldsymbol{C}_{z3})\hat{x}_3 + \boldsymbol{B}_{o3} \boldsymbol{K}_b y_c + \boldsymbol{G}_3 z_3, \qquad \hat{y}_3 = \boldsymbol{C}_{o3} \hat{x}_3$$

where $\boldsymbol{C}_{o3} \in \Re^{m_y \times n}$ with zeros in the rows corresponding to states not output by observer 3. $\boldsymbol{G}_3 =$ observer gains.

Output feedback:

$$\hat{y} = \hat{y}_1 + \hat{y}_2 + \hat{y}_3$$

Figure 2 shows an equivalent system with unity feedback. It is relatively simple to derive the state-space representation for the system in Fig. 2 as

$$\dot{x}_e = \boldsymbol{A}_e x_e + \boldsymbol{B}_e y_c$$
$$y = \begin{bmatrix} \boldsymbol{C}_y & \boldsymbol{0}_{m_y \times (n_a + n_{o1} + n_{o2} + n_{o3})} \end{bmatrix} x_e + [\boldsymbol{D}_y \boldsymbol{K}_b] y_c \quad x_e = \begin{bmatrix} x \\ x_a \\ \hat{x}_1 \\ \hat{x}_2 \\ \hat{x}_3 \end{bmatrix} \quad (5)$$
$$\hat{y} = \boldsymbol{C}_e x_e$$

where

$$\boldsymbol{A}_e = \begin{bmatrix} \boldsymbol{A} & \boldsymbol{B}\boldsymbol{C}_a & \boldsymbol{0}_{n \times n_{o1}} & \boldsymbol{0}_{n \times n_{o2}} & \boldsymbol{0}_{n \times n_{o3}} \\ \boldsymbol{0}_{n_a \times n} & \boldsymbol{A}_a & \boldsymbol{0}_{n_a \times n_{o1}} & \boldsymbol{0}_{n_a \times n_{o2}} & \boldsymbol{0}_{n_a \times n_{o3}} \\ \boldsymbol{G}_1\boldsymbol{C}_{z1} & \boldsymbol{G}_1\boldsymbol{D}_{z1}\boldsymbol{C}_a & (\boldsymbol{A}_{o1} - \boldsymbol{G}_1\boldsymbol{C}_{z1}) & \boldsymbol{0}_{n_{o1} \times n_{o2}} & \boldsymbol{0}_{n_{o1} \times n_{o3}} \\ \boldsymbol{G}_2\boldsymbol{C}_{z2} & \boldsymbol{G}_2\boldsymbol{D}_{z2}\boldsymbol{C}_a & \boldsymbol{0}_{n_{o2} \times n_{o1}} & (\boldsymbol{A}_{o2} - \boldsymbol{G}_2\boldsymbol{C}_{z2}) & \boldsymbol{0}_{n_{o2} \times n_{o3}} \\ \boldsymbol{G}_3\boldsymbol{C}_{z3} & \boldsymbol{G}_3\boldsymbol{D}_{z3}\boldsymbol{C}_a & \boldsymbol{0}_{n_{o3} \times n_{o1}} & \boldsymbol{0}_{n_{o3} \times n_{o2}} & (\boldsymbol{A}_{o3} - \boldsymbol{G}_3\boldsymbol{C}_{z3}) \end{bmatrix}$$

$$\boldsymbol{B}_e = \begin{bmatrix} \boldsymbol{B}\boldsymbol{D}_a\boldsymbol{K}_b \\ \boldsymbol{B}_a\boldsymbol{K}_b \\ \boldsymbol{B}_{o1}\boldsymbol{K}_b + \boldsymbol{G}_1\boldsymbol{D}_{z1}\boldsymbol{D}_a\boldsymbol{K}_b \\ \boldsymbol{B}_{o2}\boldsymbol{K}_b + \boldsymbol{G}_2\boldsymbol{D}_{z2}\boldsymbol{D}_a\boldsymbol{K}_b \\ \boldsymbol{B}_{o3}\boldsymbol{K}_b + \boldsymbol{G}_3\boldsymbol{D}_{z3}\boldsymbol{D}_a\boldsymbol{K}_b \end{bmatrix}$$

$$\boldsymbol{C}_e = \begin{bmatrix} \boldsymbol{0}_{m_y \times n} & \boldsymbol{0}_{m_y \times n_a} & \boldsymbol{C}_{o1} & \boldsymbol{C}_{o2} & \boldsymbol{C}_{o3} \end{bmatrix}$$

It is instructive to examine the transfer functions $(\hat{y}/y_c)(s)$ and compare them with both the original nominal plant transfer functions with no actuator and the plant with the actuator. Figure 3 shows the Bode plots of $(\hat{y}/y_c)(s)$ for the ICE vehicle, where $y = \alpha =$ angle of attack. The nominal plant transfer function is shown along with the observed feedback signal for various observer bandwidths. Several observations are worth noting. First of all, although the addition of actuator dynamics (with no observer) changes the apparent relative order for the SMC, the apparent relative order of the observed signal is the same as the nominal plant with no actuators. This is important because the order of the sliding manifold is one less than the relative order of the plant and is not tolerant to changes in relative order. Second, fast observers (those with eigenvalues far into the left half-plane) display a characteristic distortion in the Bode magnitude curve of $(\hat{y}/y_c)(s)$ near the frequency of the actuator dynamics and a large increase in phase lag. Third, by slowing down the observer, the distortion in the magnitude curve and the large phase lag can be greatly reduced. This can be used to help determine the best observer gains. Similar Bode plots are examined for each controlled variable in the square system architecture.

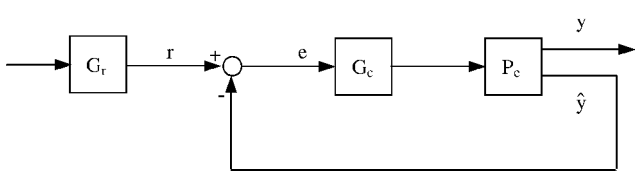

Fig. 2 Unity feedback equivalent of Fig. 1.

Model Reference Hedging

Observer-based SMC helps deal with the problem of unmodeled parasitic dynamics. However, the addition of the observer does not directly address the issue of control saturation. The observer does help with rate saturation to some degree because of phase lag reductions at medium to high frequencies. However, position saturation is still an issue, especially when the system does not have redundant control effectors. Initially, in an attempt to deal with control saturation, a method called model reference hedging was pursued. The concept of hedging has been successfully demonstrated in a dynamic inversion design approach.[26] In other words, "[t]he reference model is moved backwards (hedged) by an estimate of the amount the plant did not move due to system characteristics the control designer does not want the adaptive control element to 'know' about."[26] The actual accelerations are subtracted from the expected accelerations (assuming no actuators). This difference represents the amount of desired acceleration that was not achieved due to the actuators and should capture nonlinear saturation of the actual actuators. This difference is then subtracted from the reference model acceleration. Because all of this is done in a dynamic inversion setting, these accelerations are pseudocommands for the dynamic inversion controller, and Johnson et al. call this "Pseudo-Control Hedging." The concept has great merit and is very successful in such applications.[26]

To employ this method in an SMC design, some modification to the implementation is required. Rather than subtracting the acceleration difference from the reference model pseudocommand, the controlled variable output is subtracted from the expected output (through a nominal system with no actuators). This signal y_h represents the amount of unachieved performance due to the presence of the actuator. The signal y_h passes through a hedge gain K_h and is subtracted directly from the second-order model reference states as shown in Fig. 4.

To investigate how hedging affects the system, an analytical expression for the system with hedging is needed. Consider, initially, a model architecture as shown in Fig. 5. In this system, the hedge

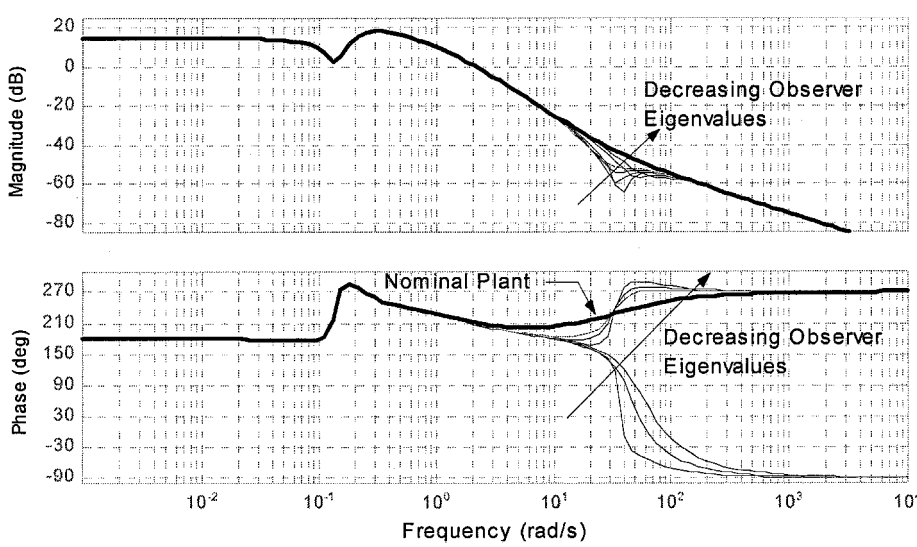

Fig. 3 Bode plots, $(\hat{\alpha}/u_{c\alpha})$, ICE, various observer eigenvalues.

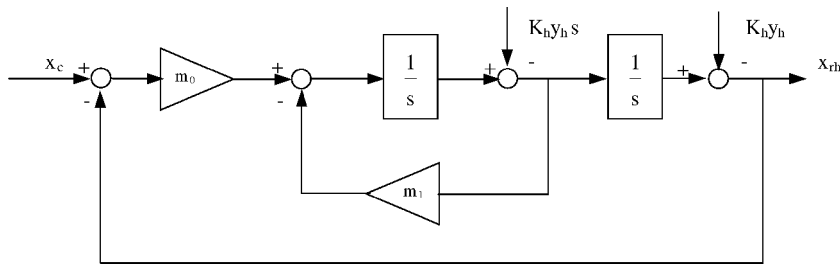

Fig. 4 Second-order hedged reference model.

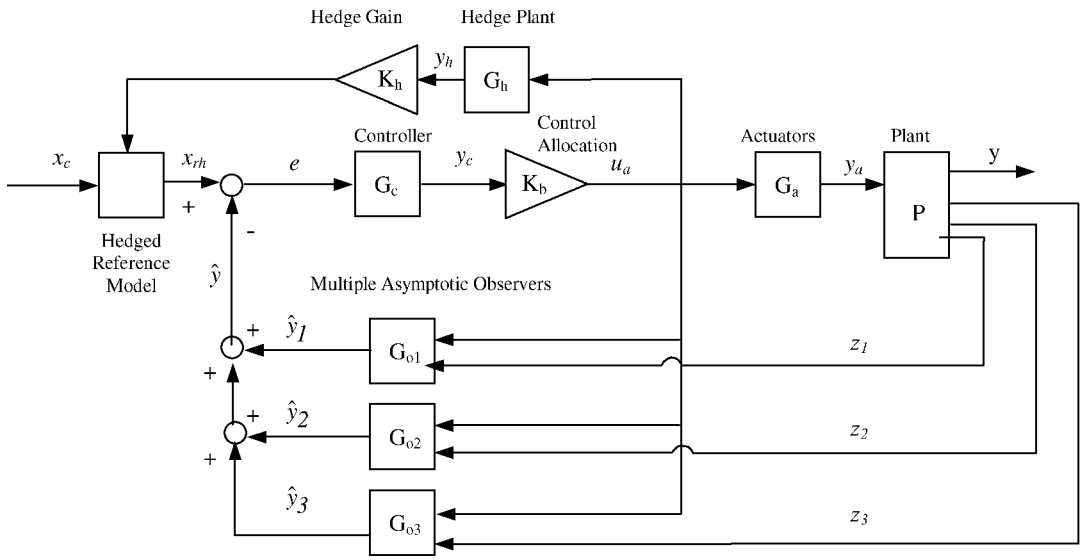

Fig. 5 Hedged system architecture.

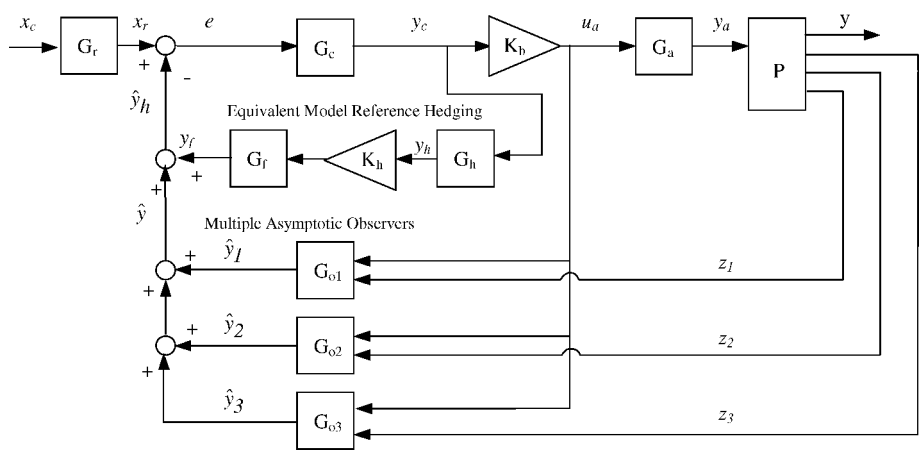

Fig. 6 Equivalent hedged system architecture.

plant G_h is simply the nominal plant model (assuming it is stable). The subsystem block labeled hedged reference model is the subsystem shown in Fig. 4. Because hedging occurs on individual control variable channels, it is possible to write the transfer function for the hedged reference model. It can be shown that this transfer function (for a second-order reference model) is given by

$$x_{rh} = \left(\frac{m_0}{s^2 + m_1 s + m_0}\right) x_c - \left(\frac{2s^2 + m_1 s}{s^2 + m_1 s + m_0}\right) K_h y_h$$

$$\equiv G_r(s) x_c - G_f(s) K_h y_h \tag{6}$$

Equation (6) indicates that the hedged reference signal consists of two parts, a reference model part and a hedge signal passing through a hedge filter, G_f. With this definition, the block diagram can be redrawn as shown in Fig. 6, with the following hedge system definitions.

Hedge plant:

$$\dot{x}_h = \boldsymbol{A}_h x_h + \boldsymbol{B}_h \boldsymbol{K}_b y_c, \qquad y_h = \boldsymbol{C}_h x_h + \boldsymbol{D}_h \boldsymbol{K}_b y_c \tag{7a}$$

Hedge filter:

$$\dot{x}_f = \boldsymbol{A}_f x_f + \boldsymbol{B}_f \boldsymbol{K}_h y_h, \qquad y_f = \boldsymbol{C}_f x_f + \boldsymbol{D}_f \boldsymbol{K}_h y_h \tag{7b}$$

Output feedback:

$$\hat{y}_h = \hat{y}_1 + \hat{y}_2 + \hat{y}_3 + y_f \tag{7c}$$

the equivalent unity feedback system (Fig. 2) is defined in state space as

$$\begin{aligned}\dot{x}_e &= \boldsymbol{A}_e x_e + \boldsymbol{B}_e y_c \\ y &= \left[\boldsymbol{C}_y \quad \boldsymbol{0}_{m_y \times (n_a + n_{o1} + n_{o2} + n_{o3} + n_f + n_h)}\right] \\ &\quad \times x_e + [\boldsymbol{D}_y \boldsymbol{K}_b] y_c \\ \hat{y}_h &= \boldsymbol{C}_e x_e + \boldsymbol{D}_e y_c\end{aligned} \qquad x_e = \begin{bmatrix} x \\ x_a \\ \hat{x}_1 \\ \hat{x}_2 \\ \hat{x}_3 \\ x_f \\ x_h \end{bmatrix} \tag{8}$$

where

$$\boldsymbol{A}_e = \begin{bmatrix} \boldsymbol{A} & \boldsymbol{B}\boldsymbol{C}_a & \boldsymbol{0}_{n \times n_{o1}} & \boldsymbol{0}_{n \times n_{o2}} & \boldsymbol{0}_{n \times n_{o3}} & \boldsymbol{0}_{n \times n_f} & \boldsymbol{0}_{n \times n_h} \\ \boldsymbol{0}_{n_a \times n} & \boldsymbol{A}_a & \boldsymbol{0}_{n_a \times n_{o1}} & \boldsymbol{0}_{n_a \times n_{o2}} & \boldsymbol{0}_{n_a \times n_{o3}} & \boldsymbol{0}_{n_a \times n_f} & \boldsymbol{0}_{n_a \times n_h} \\ \boldsymbol{G}_1\boldsymbol{C}_{z1} & \boldsymbol{G}_1\boldsymbol{D}_{z1}\boldsymbol{C}_a & (\boldsymbol{A}_{o1} - \boldsymbol{G}_1\boldsymbol{C}_{z1}) & \boldsymbol{0}_{n_{o1} \times n_{o2}} & \boldsymbol{0}_{n_{o1} \times n_{o3}} & \boldsymbol{0}_{n_{o1} \times n_f} & \boldsymbol{0}_{n_{o1} \times n_h} \\ \boldsymbol{G}_2\boldsymbol{C}_{z2} & \boldsymbol{G}_2\boldsymbol{D}_{z2}\boldsymbol{C}_a & \boldsymbol{0}_{n_{o2} \times n_{o1}} & (\boldsymbol{A}_{o2} - \boldsymbol{G}_2\boldsymbol{C}_{z2}) & \boldsymbol{0}_{n_{o2} \times n_{o3}} & \boldsymbol{0}_{n_{o2} \times n_f} & \boldsymbol{0}_{n_{o2} \times n_h} \\ \boldsymbol{G}_3\boldsymbol{C}_{z3} & \boldsymbol{G}_3\boldsymbol{D}_{z3}\boldsymbol{C}_a & \boldsymbol{0}_{n_{o3} \times n_{o1}} & \boldsymbol{0}_{n_{o3} \times n_{o2}} & (\boldsymbol{A}_{o3} - \boldsymbol{G}_3\boldsymbol{C}_{z3}) & \boldsymbol{0}_{n_{o3} \times n_f} & \boldsymbol{0}_{n_{o3} \times n_h} \\ \boldsymbol{0}_{n_f \times n} & \boldsymbol{0}_{n_f \times n_a} & \boldsymbol{0}_{n_f \times n_{o1}} & \boldsymbol{0}_{n_f \times n_{o2}} & \boldsymbol{0}_{n_f \times n_{o3}} & \boldsymbol{A}_f & \boldsymbol{B}_f\boldsymbol{K}_h\boldsymbol{C}_h \\ \boldsymbol{0}_{n_h \times n} & \boldsymbol{0}_{n_h \times n_a} & \boldsymbol{0}_{n_h \times n_{o1}} & \boldsymbol{0}_{n_h \times n_{o2}} & \boldsymbol{0}_{n_h \times n_{o3}} & \boldsymbol{0}_{n_h \times n_f} & \boldsymbol{A}_h \end{bmatrix}$$

$$\boldsymbol{B}_e = \begin{bmatrix} \boldsymbol{B}\boldsymbol{D}_a\boldsymbol{K}_b \\ \boldsymbol{B}_a\boldsymbol{K}_b \\ \boldsymbol{B}_{o1}\boldsymbol{K}_b + \boldsymbol{G}_1\boldsymbol{D}_{z1}\boldsymbol{D}_a\boldsymbol{K}_b \\ \boldsymbol{B}_{o2}\boldsymbol{K}_b + \boldsymbol{G}_2\boldsymbol{D}_{z2}\boldsymbol{D}_a\boldsymbol{K}_b \\ \boldsymbol{B}_{o3}\boldsymbol{K}_b + \boldsymbol{G}_3\boldsymbol{D}_{z3}\boldsymbol{D}_a\boldsymbol{K}_b \\ \boldsymbol{B}_f\boldsymbol{K}_h\boldsymbol{D}_h\boldsymbol{K}_b \\ \boldsymbol{B}_h\boldsymbol{K}_b \end{bmatrix}$$

$$\boldsymbol{C}_e = [\boldsymbol{0}_{m_y \times n} \quad \boldsymbol{0}_{m_y \times n_a} \quad \boldsymbol{C}_{o1} \quad \boldsymbol{C}_{o2} \quad \boldsymbol{C}_{o3} \quad \boldsymbol{C}_f \quad \boldsymbol{D}_f\boldsymbol{K}_h\boldsymbol{C}_h]$$

$$\boldsymbol{D}_e = \boldsymbol{D}_f\boldsymbol{K}_h\boldsymbol{D}_h\boldsymbol{K}_b$$

Now the effects of hedging can be examined on the Bode plots of the transfer functions $(\hat{y}_h/y_c)(s)$ as was done with the observer. After the examination of several different systems, it was noted that the hedge signal has basically the same loop shape for each system. It resembles a derivative at low frequencies; it peaks, and then rolls off at the relative order of the plant at high frequencies. This is not surprising considering the hedge filter has the same form in all cases: It resembles a high-pass filter. All real plants have a high-frequency roll-off. When these two are placed in series, the result is a characteristic convex shape. The question then is this: Can the same beneficial effects of hedging be achieved with a simplified "equivalent hedge" transfer function? This is highly desirable because, in its current form, hedging can only be used with a stable plant.

Consider a hedge filter of the form (a high-pass filter)

$$G_f(s) = s/(s + a_f) \tag{9}$$

and a hedge plant of the form (a low-pass filter)

$$G_h(s) = b_h \Big/ \left(s^2 + a_h s + b_h\right) \tag{10}$$

The hedge plant G_h in Eq. (10) has relative order two and is intended to be used with a system with a relative order of one. The extra pole is added to have additional high-frequency roll-off. In general, the simplified model can be designed to be close to the original hedge system and will achieve the same desired effects. Note, the actuator states are not required as they are in pseudocommand hedging.[26] The following technique is proposed for creating the hedge model. Begin by plotting the Bode plots of $(\hat{y}_h/y_c)(s)$ and the nominal system as before, with zero hedge gain. The basic form of the desired hedge model loop shape is as follows: 1) +20 dB/decade slope at low frequencies, 2) $-20 \cdot r$ dB/decade slope at frequencies where the actuators distort the magnitude curve (where r is the relative degree of nominal system with no actuators), and 3) $-20 \cdot r - 20$ dB/decade slope at high frequencies.

The desired hedge signal loop shape can be created (for a system with relative order one) using the hedge plant and hedge filter given in Eqs. (9) and (10). The pole in the hedge filter is placed at the high-frequency end of the magnitude distortion and the two poles of the hedge plant are placed at the low-frequency end of the distortion. A conceptual example of this is illustrated in Fig. 7. With the correct loop shape, the hedge gain is then adjusted to minimize error in the phase plot and the distortion in the magnitude plot. If the observer is very fast, or if no observer is used, there is a minimum hedge gain that will stabilize the system. By the use of this method of examining the Bode plots of $(\hat{y}_h/y_c)(s)$, it is easy to determine the minimum hedge gain. Examining the Bode plots will also give an indication of the upper limit for this gain. In general, if the hedge signal moves the magnitude plot of $(\hat{y}_h/y_c)(s)$ above the nominal plant magnitude plot, the closed-loop system will have unacceptable overshoot and phase lag. This can lead to instability if outer control loops are closed around the SMC system.

In MIMO applications, the cross-coupled transfer functions need to be examined as well. If cross-coupling effects are strong, the interaction of the command for one channel with the unmodeled parasitic dynamics can lead to instability in another channel. Therefore, if necessary, a hedge model for the cross-coupling term can be designed and the feedback loop properly shaped. The same guidelines just introduced are also used for the cross-coupled hedge models. This cross-term hedge signal is then added to the primary hedge signal.

Note that the proposed hedging method no longer resembles the concept of hedging given in the initial reference work.[26] Note in Fig. 6 that all of the hedge signal dynamics occur in parallel with the observer loop and no longer enter the reference model. The hedging method here is really a form of observer loop shaping. In fact, this approach is similar to loop transfer recovery as used in linear quadratic gaussian control in which optimality of the observer is traded for increased stability margins. The hedge signal used here

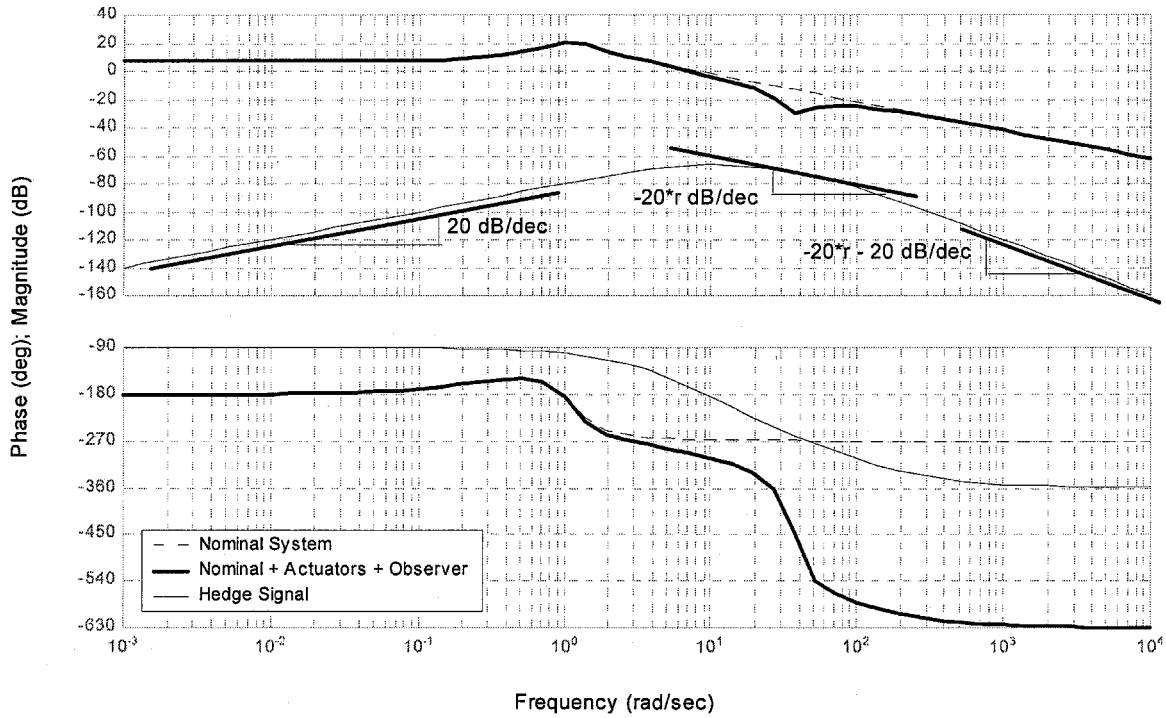

Fig. 7 Creating the hedge model, ($\hat{y}_h/y_c$).

also has the effect of tuning down the observer at certain frequencies to recover desirable stability margins. It can also be shown that the hedge system is attempting to invert the actuator dynamics. This is why it is highly dependent on the actuator bandwidths. When viewed in this light, one could argue that this is simply another form of an SMC prefilter-type design.[13]

The preceding discussion was an attempt to illustrate the effectiveness of model reference hedging and has demonstrated a design procedure, all in the frequency domain. Observers and hedging in the feedback paths allow the SMC to see the plant (nearly) without parasitic dynamics. Thus, some of the performance and robustness of the SMC design approach are recovered. Unfortunately, rigorous proofs that quantify stability and robustness for nonlinear applications are, as yet, unavailable.

Frequency-Domain SMC Design Procedure

The following technique is based on the design approach offered in earlier applications[14,15]:

1) The vehicle model is obtained, along with an estimate of the frequency beyond which parasitic dynamics (or unstructured uncertainties) are likely to come into play. This frequency is referred to as the limit frequency in this discussion. Actuator dynamics are not included in the nominal plant model.

2) A reference model is chosen for each control variable channel. Because piloted flight control is of interest in the present application, this reference model should be selected with an eye toward level 1 handling qualities with no pilot-induced oscillation (PIO) tendencies. This can be accomplished based on pilot model-based handling qualities and the PIO prediction technique.[27,28]

3) The desired feedback structure of the control system is determined with a square system architecture. For example, if a roll-rate command flight-control system is desired, then roll rate p_c becomes the output of the reference model, and estimated roll rate $\hat{p}$ is fed back to the SMC system from the observer. System error is then defined as $e(t) = p_c(t) - \hat{p}(t)$. Special care must be given to ensure that the dynamics of the uncontrolled variables remain stable and no non-minimum phase transmission zeros exist. Also, if there are redundant control effectors for the desired moments/pseudocommands, a control distribution matrix must be defined.

4) The sliding manifold σ is chosen based on the following principles:

a) From a tracking error expression, σ is derived as

$$\sigma = e(t)^{p-1} + K_{p-2}e(t)^{p-2} + \cdots + K_0 e(t) + K_{-1}\int e(t)\,\mathrm{d}t \tag{11}$$

where p is the relative order of the system, that is, the number of times the vehicle output must be differentiated for the input to appear. Note that the $p-1$ derivative of the error signal is included in the definition of σ. An integral term also appears in Eq. (11) to counter the steady-state bias often created with the use of a boundary layer.

b) Recognizing that a boundary layer is to be implemented, the control law is expressed as a linear transfer function, assuming the boundary layer is large enough to remain within the linear region of the saturation element:

$$u(s) = (\rho/\varepsilon)\sigma$$

$$= K_\rho\left[s^{p-1} + K_{p-2}s^{p-2} + \cdots + K_0 + (K_{-1}/s)\right]e(s) \tag{12}$$

The parameters K_i are chosen to provide desirable properties in the frequency domain. This means creating a loop transmission with broad K/s-like characteristics around crossover.[29] This will always be possible because enough derivatives are included in Eq. (12) to create exact K/s characteristics beyond a certain frequency (at least as high as the limit frequency). Parasitic dynamics are deliberately excluded in this formulation. This step will involve obtaining an estimate of K_ρ because this value will determine the crossover frequency of the loop transmission. This crossover frequency is selected to provide acceptable stability margins as obtained from a Bode plot of the loop transmission, but using a value of K_ρ at least as large as the largest amplitude limit of any of the control effectors. The latter criterion is included to accommodate maximum trim positions of the control effectors. As opposed to typical designs involving loop shaping, very high crossover frequencies may result from this step. Indeed, these frequencies may be well beyond the limit frequency. This result is of no immediate concern. If a MIMO

system is being designed, a classic sequential loop closure technique is used, thereby sequentially and independently determining the coefficients for each sliding manifold.

5) By the use of the K_i just determined in the definition of the sliding function, the existence of a sliding mode is verified in the inner loops using a true SMC. This step is completed without the observer, actuators, reference model, or pilot model, that is, under the assumption that no outer loop is being utilized. If necessary, ρ is increased until sliding behavior is created. The initial value of $\rho = K_\rho$ obtained in step 4b should be considered a lower limit in this process. Although an analytical approach to determine ρ is certainly possible here, a more expedient route of establishing the sliding mode using a computer simulation of the system is also possible. Near-perfect tracking in the face of large parameter variations should be observed. The control signal, however, will exhibit very high-frequency switching.

6) A boundary layer is included in the controller by replacing the signum function $\text{sgn}(\sigma)$ with the saturation function $\text{sat}(\sigma/\varepsilon)$. While maintaining an approximate constant $\rho/\varepsilon = K_\rho$, increase the boundary layer thickness ε until no high-frequency switching is evident. Again, a simulation of the SMC system is a convenient way of finding this ε. Near-perfect tracking (with a continuous control signal) in the face of large parameter variations should be observed.

7) Parasitic dynamics are included in the model. The SMC controller will very likely be unstable at this juncture.

8) An asymptotic observer is created for each control variable channel as was discussed.

9) A hedge model is designed as described earlier.

10) The frequency domain characteristics of the open- and closed-loop SMC system with observer, boundary layer, and reference model are examined to ensure that stability of the linear system is in evidence.

Design Example: ICE MIMO Linear Six-Degree-of-Freedom Model

ICE Vehicle

The ICE aircraft model has been developed by Lockheed-Martin, Fort Worth, Texas, under a U.S. Air Force Research Laboratories (AFRL) sponsored program[30] and is the vehicle of choice for many controls applications in the current literature.[1,2,11,23,31–36] It is a single-engine, multirole, supersonic, tailless fighter aircraft with a 65-deg sweep delta wing (Fig. 8). The conventional control effectors include elevons, symmetric pitch flaps, and outboard leading-edge flaps. The innovative control effectors include pitch and yaw thrust vectoring, all-moving tips, and spoiler slot deflectors. The all-moving tips and spoiler slot deflectors have zero lower deflection limits.

The static aerodynamic force and moment data were collected by NASA Langley Research Center and AFRL using wind-tunnel tests with a 1/18th scale model. Additional wind-tunnel tests during phase 2 of the ICE program provide updated data for simulation models.[1] There are strong multi-axis effects and highly nonlinear interactions between the close-coupled control surfaces. The full nonlinear simulation of the ICE vehicle is proprietary; however, linearized models at various flight conditions (that do not include nonlinear effector interactions) have been made available to this research directly from the NASA Langley Research Center.

SMC Design

The SMC design considers simultaneous control of longitudinal and lateral degrees of freedom. The response variables are angle of attack α, roll rate about the velocity vector p_s, and sideslip β. Decoupled tracking performance is desired:

1) The flight condition used for this study is 1 g, wings-level, Mach 0.3, altitude of 15,000 ft (4572 m). The linearized model for this flight condition contains 8 states, 11 outputs, and 11 control inputs. The open-loop plant is unstable and highly coupled.

2) Reference models for each response variable are created as well-damped second-order systems with dynamics predicted to yield level 1 handling qualities with no PIO tendencies. The methodology utilizing a pilot structural model is employed.[27] The reference models so obtained are

$$G_\alpha(s) = (\alpha_r/\alpha_c)(s) = 100/(s^2 + 20s + 100)$$

$$G_p(s) = (p_r/p_c)(s) = 100/(s^2 + 20s + 100)$$

$$G_\beta(s) = (\beta_r/\beta_c)(s) = 100/(s^2 + 25s + 100) \qquad (13)$$

3) A square system architecture is defined as shown in Fig. 9. As shown, the feedback structure of the flight-control system consists of angle of attack command and hold, roll-rate command, and sideslip command and hold. Analytical models of the human pilot controlling the angle of attack (α) and roll-attitude (ϕ) loops are developed and included in the Simulink simulation of the pilot/vehicle system.[27] A common crossover frequency of 1.5 rad/s is chosen for the α and ϕ loops. The β loop is not closed by the pilot. It is assumed that the pilot flies the vehicle with "feet on the floor." The controller to be designed generates pseudocommands for angle of attack, stability axis roll rate, and sideslip angle. These demands are allocated to the 11 control effectors using a pseudoinverse approach.[37] If the preferred actuator positions are assumed to be zero, the solution to the control allocation problem using a pseudoinverse is

$$\boldsymbol{B}_k = \boldsymbol{W}_u^{-1}\boldsymbol{B}^T\left(\boldsymbol{B}\boldsymbol{W}_u^{-1}\boldsymbol{B}^T\right)^{-1} \qquad (14)$$

where the weighting matrix $\boldsymbol{W}_u$ is assumed to be the identity matrix. The resulting control distribution matrix $\boldsymbol{B}_k$ is an 11×3 matrix with constant elements. Noncorrelated sum-of-sines inputs serve as tracking commands to the pilot in the ϕ and α loops. β command is zero.

4) The system (without actuators) has a relative order of one for all three control variables. Therefore, the forms of the sliding manifolds are

$$\sigma = K_0 e + K_{-1}\int e\,\mathrm{d}\tau, \qquad e = \{(\alpha_r - \hat{\alpha}), (p_r - \hat{p}), (\beta_r - \hat{\beta})\}^T \qquad (15)$$

The control laws, under the assumption of the use of a boundary layer, can then be expressed in linear form, resulting in one zero to be placed and a gain to be set for each loop during the loop-shaping design. By the use of a traditional sequential loop-shaping technique, the parameters of Eq. (15) are determined, with roll rate being the first loop to be closed, followed by α, and then β. The designed manifolds are given in Eq. (16). A crossover frequency of

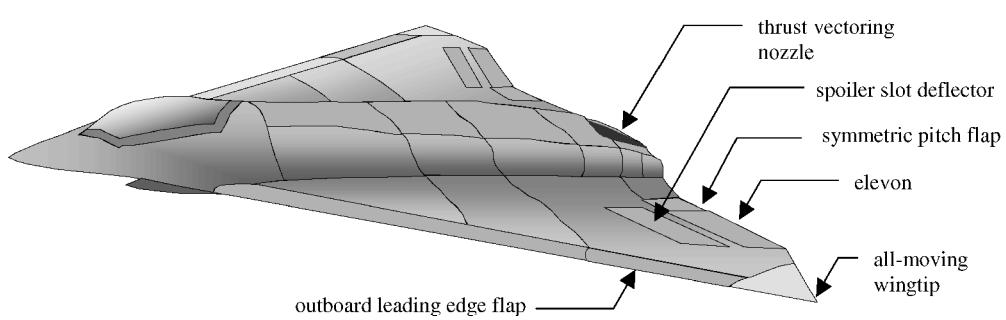

Fig. 8 ICE vehicle.

$\omega = 1000$ rad/s is set for each channel.

$$u_{c\alpha}(s) = 5000[(s+10)/s], \qquad u_{cp}(s) = 1000[(s+20)/s]$$
$$u_{c\beta}(s) = 5000[(s+10)/s] \tag{16}$$

5) Sliding behavior is verified by simulation. As expected, the SMC provides near-perfect tracking and is invariant to the system parameter changes. The control output shows the classic high-frequency switching. The controller achieves decoupled tracking of α, p_s, and β, as desired.

6) Next, the boundary layer is increased until a continuous control signal is achieved. For this model, $\varepsilon = 1$ is chosen for all three channels. Again, the performance is excellent, even in the face of large system failures.

7) The next step is the inclusion of the actuators. The actuators are second order with rate and position limits. As expected, the nominal system immediately goes unstable.

8) and 9) The next steps are to design the observers and hedge models. In this procedure, the eigenvalues of the observers are chosen to be real and nearly identical. By the use of the frequency domain approach introduced earlier, it is seen that (without hedging) the α-channel observer must have eigenvalues of 10 rad/s or less, the p-channel observer can have eigenvalues as large as 100 rad/s, and the β channel must have eigenvalues of 5 rad/s or less. It appears that hedging will help in the α channel, is unnecessary in the p channel, and is probably required in the β channel. Three cross-coupling hedge models were found to be necessary in the design. The parameters chosen for the observer and hedging models are shown in Table 1. The design Bode plots for each primary channel are given in Figs. 10–12.

Simulation Results

To illustrate the robustness of the observer-based SMC design, the system is exercised with measurement noise, system failure, and the pilot model in the loop. The Simulink simulation is run with an ODE2 solver using a fixed time step of $\Delta t = 0.0005$ s. Vehicle failure occurs at $t = 20$ s. Vehicle failure is defined as follows:

1) Vehicle failure may be defined as plant failure. ($\boldsymbol{A}$ matrix is multiplied by two, with the exception of the elements describing kinematic relationships; $\boldsymbol{B}$ matrix is multiplied by 0.75.)

2) All actuators experience a 50-ms time delay.

3) Left elevon rate limits are reduced from 150 to 10 deg/s; position limits are reduced from ± 30 to ± 15 deg.

4) Symmetric pitch flap undamped natural frequency is reduced from 63 to 10 rad/s.

5) Left leading-edge flap is jammed at +5 deg.

6) Pitch nozzle actuator undamped natural frequency is reduced from 39 to 10 rad/s.

7) Yaw nozzle actuator undamped natural frequency is reduced from 39 to 10 rad/s.

The resulting outer-loop tracking is shown in Fig. 13. After system failure, tracking is noticeably degraded, but the vehicle remains stable. The actuator deflections are not shown, however, it is seen that nearly all of the actuators are in nearly constant rate saturation after the failure.

A more classic loop-shape design was created for comparison. Three forward-loop compensators were synthesized as

$$\frac{u_{c\alpha}}{\alpha_e} = \frac{56(s^2+1.7s+0.52)}{s^2+32s}, \qquad \frac{u_{cp}}{p_e} = \frac{10(s^2+0.4s+0.04)}{s^2}$$
$$\frac{u_{c\beta}}{\beta_e} = \frac{50(s^2+2s+1)}{s^2+50s} \tag{17}$$

As Fig. 14 indicates, this design goes unstable shortly after the failure occurs.

Predictions of handling qualities and PIO susceptibility for the SMC system after the failure can be made using the pilot/vehicle analysis technique.[27,38] By the use of this technique, level 1 handling qualities are still predicted for the α-tracking task, with predicted PIO ratings less than or equal to two. Level 2 handling qualities are predicted for the ϕ-tracking task, with predicted PIO ratings between two and four. In view of these results, certain observations

Table 1 Observer and hedge models for ICE

Channel	Model
	Observer poles
α	$\lambda = -10.0, -10.1, -10.2, -10.3, -10.4, -10.5, -10.6, -10.7$
p_s	$\lambda = -40.0, -40.1, -40.2, -40.3, -40.4, -40.5, -40.6, -40.7$
β	$\lambda = -1.0, -1.1, -1.2, -1.3, -1.4, -1.5, -1.6, -1.7$
	Hedge model
$\alpha_h/u_{c\alpha}$	$[s/(s+10)][4/(s^2+4s+4)]$
p_h/u_{cp}	$[s/(s+50)][4/(s^2+4s+4)]$
$\beta_h/u_{c\beta}$	$[s/(s+5)][2/(s^2+3s+2)]$
$\alpha_h/u_{c\beta}$	$0.0001[s/(s+10)][4/(s^2+4s+4)]\,\alpha$ cross term
$p_h/u_{c\beta}$	$-0.2[s/(s+50)][64/(s^2+16s+64)]\,p_s$ cross term
β_h/u_{cp}	$0.02[s/(s+5)][1/(s^2+2s+1)]\,\beta$ cross term
	Hedge gain
α	1.0
p_s	2.0
β	10.0

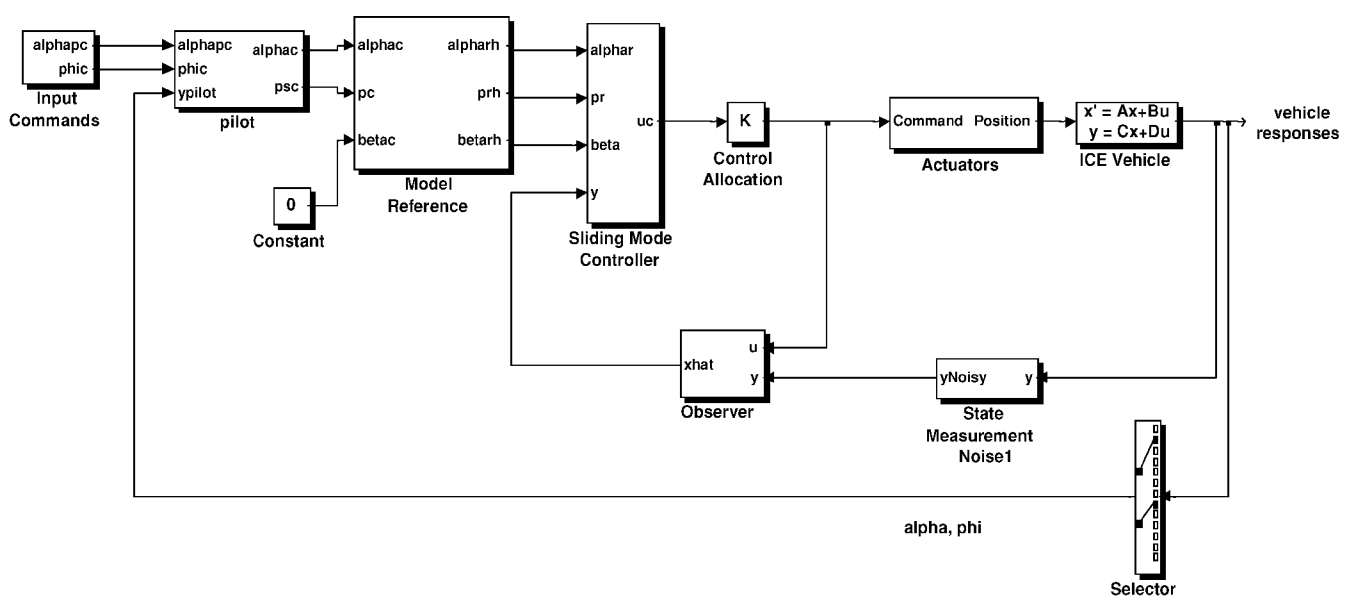

Fig. 9 Simulink diagram of the ICE pilot/vehicle/SMC system.

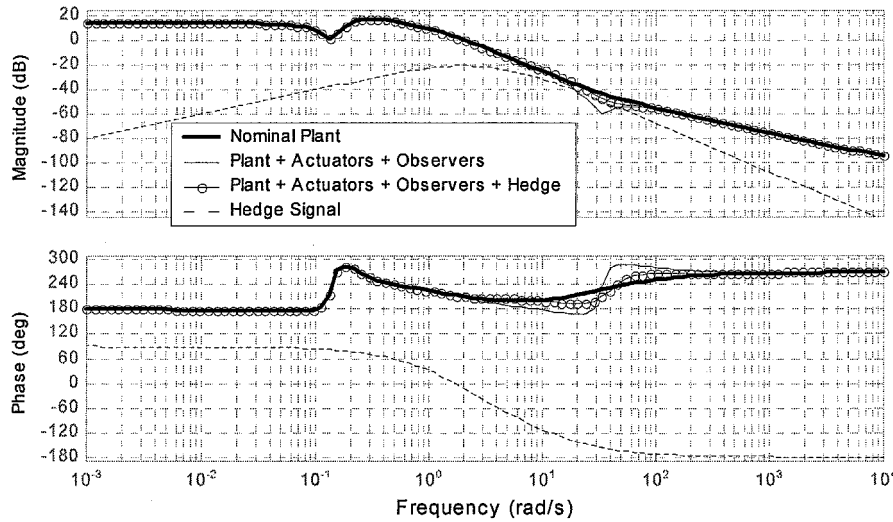

Fig. 10 Bode plots, ($\hat{\alpha}_h/u_{c\alpha}$), ICE hedge design.

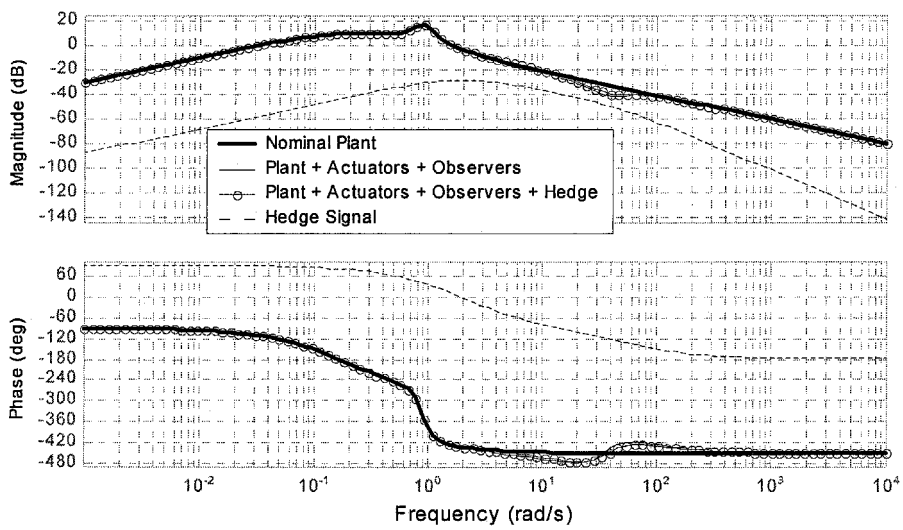

Fig. 11 Bode plots, ($\hat{p}_h/u_{cp}$), ICE hedge design.

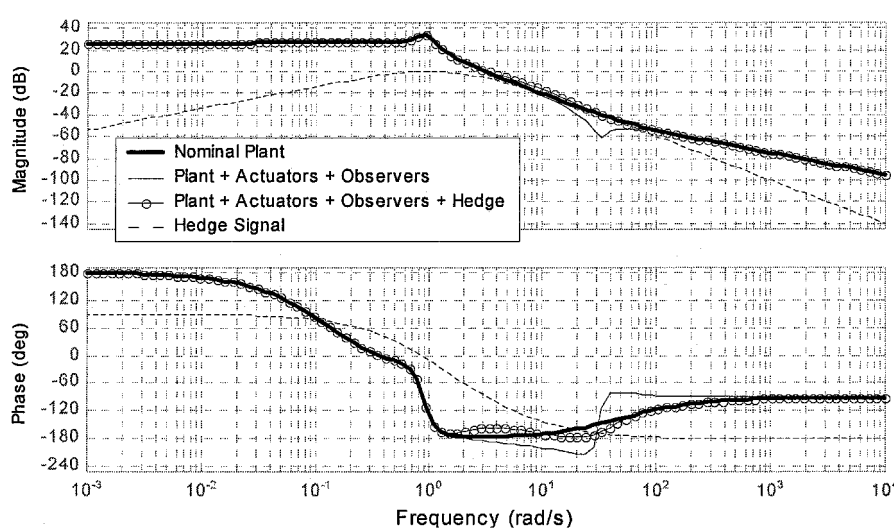

Fig. 12 Bode plots, ($\hat{\beta}_h/u_{c\beta}$), ICE hedge design.

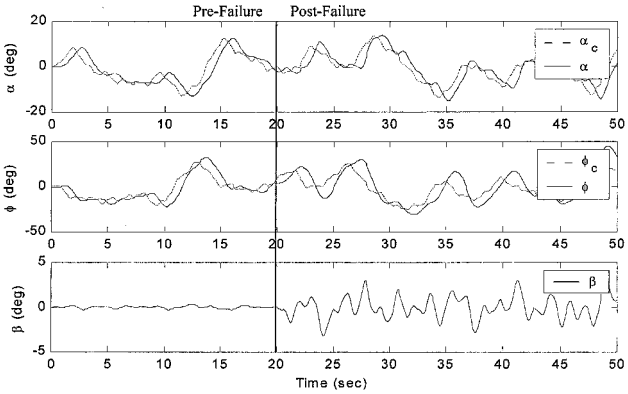

Fig. 13 Outer-loop tracking (α, ϕ, and β), ICE, with SMC, actuators, observers, hedging, and noise, failure at $t = 20$ s.

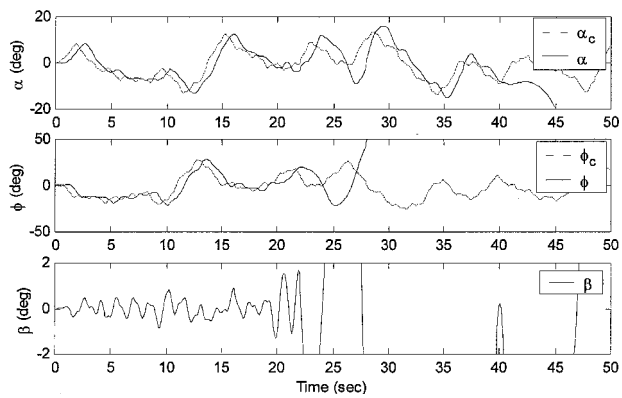

Fig. 14 Outer-loop tracking (α, ϕ, and β), ICE, with loop-shaped controller, actuators, and noise, failure at $t = 20$ s.

are in order. First of all, this is a significant system failure, and it is remarkable that the controller is able to maintain stability. Second, the input maneuvers are very aggressive. After a failure of this magnitude, a pilot would not be commanding such a demanding profile. Third, the handling qualities and pilot-induced oscillation level predictions assume a static pilot model. In actuality, a real pilot would compensate for the perceived change in vehicle dynamics. Therefore, the results shown are conservative.

Conclusions

Using asymptotic observers with sliding mode control has been shown to help mitigate the adverse effects of parasitic dynamics, and a design method for choosing observer gains has been presented. A form of model reference hedging has been shown to be equivalent to an SMC prefilter that helps shape the feedback loop, thus, partially removing the effects of actuator dynamics. A complete design procedure has been presented that incorporates a frequency domain approach to select 1) the sliding manifold, 2) the observer eigenvalues, and 3) the hedging dynamics. The approach was successfully applied to the design of a flight-control system for a model of the ICE fighter aircraft. Stability and performance robustness were demonstrated in the presence of significant actuator degradation and variation in vehicle dynamics.

Acknowledgments

This research was supported by Grant NCC1-01010 from NASA Langley Research Center. Barton Bacon serves as the Grant Technical Manger. Support was also provided by the U.S. Air Force in sponsoring S. R. Wells's graduate studies.

References

[1]Eberhardt, R. L., and Ward, D. G., "Indirect Adaptive Flight Control of a Tailless Fighter Aircraft," AIAA Paper 99-4042, Aug. 1999.

[2]Eberhardt, R. L., and Ward, D. G., "Indirect Adaptive Flight Control Interactions," *International Journal of Robust and Nonlinear Control*, Vol. 9, No. 14, 1999, pp. 1013–1031.

[3]Pachter, M., Chandler, P. R., and Mears, M., "Reconfigurable Tracking Control with Saturation," *Journal of Guidance, Control, and Dynamics*, Vol. 18, No. 5, 1995, pp. 1016–1022.

[4]Ward, D. G., and Barron, R., "A Self-Designing Receding Horizon Optimal Flight Controller," *Proceedings of American Control Conference*, Vol. 5, IEEE Publications, Piscataway, NJ, 1995, pp. 3490–3494.

[5]Ward, D. G., Monaco, J. F., and Schierman, J. D., "Reconfigurable Control for VTOL UAV Shipboard Landing," AIAA Paper 99-4046, Aug. 1999.

[6]Maybeck, P. S., "Multiple Model Adaptive Algorithms for Detecting and Compensating Sensor and Actuator/Surface Failures in Aircraft Flight Control Systems," *International Journal of Robust and Nonlinear Control*, Vol. 9, No. 14, 1999, pp. 1051–1070.

[7]Maybeck, P. S., and Stevens, R. D., "Reconfigurable Flight Control via Multiple Model Adaptive Control Methods," *IEEE Transactions on Aerospace and Electronic Systems*, Vol. 27, No. 3, 1991, pp. 470–480.

[8]Brinker, J. S., and Wise, K. A., "Nonlinear Simulation Analysis of a Tailless Advanced Fighter Aircraft Reconfigurable Flight Control Law," AIAA Paper 99-4040, Aug. 1999.

[9]Brinker, J. S., and Wise, K. A., "Flight Testing of a Reconfigurable Control Law on the X-36 Tailless Fighter Aircraft," *Journal of Guidance, Control, and Dynamics*, Vol. 24, No. 5, 2001, pp. 903–909.

[10]Wise, K. A., Brinker, J. S., Calise, A. J., Enns, D. F., Elgersma, M. R., and Voulgaris, P. G., "Direct Adaptive Reconfigurable Flight Control for a Tailless Advanced Fighter Aircraft," *International Journal of Robust and Nonlinear Control*, Vol. 9, No. 14, 1999, pp. 999–1012.

[11]Schumacher, C., "Adaptive Flight Control Using Dynamic Inversion and Neural Networks," AIAA Paper 99-4086, Aug. 1999.

[12]Calise, A. J., Lee, S., and Sharma, M., "Development of a Reconfigurable Flight Control Law for a Tailless Aircraft," *Journal of Guidance, Control, and Dynamics*, Vol. 24, No. 5, 2001, pp. 896–902.

[13]Young, K. D., Utkin, V. I., and Özgüner, Ü., "A Control Engineer's Guide to Sliding Mode Control," *IEEE Transactions on Control Systems Technology*, Vol. 7, No. 3, 1999, pp. 328–342.

[14]Hess, R. A., and Wells, S. R., "Sliding Mode Control Applied to Reconfigurable Flight Control Design," *Journal of Guidance, Control, and Dynamics* (to be published).

[15]Hess, R. A., Wells, S. R., and Vetter, T. K., "MIMO Sliding Mode Control as an Alternative to Reconfigurable Flight Control Designs," *Proceedings of American Control Conference*, IEEE Publications, Piscataway, NJ, 2002, pp. 3637–3644.

[16]DeCarlo, R. A., Zak, S. H., and Drakunov, S. V., "Section 57.5: Variable Structure, Sliding Mode Design," *The Control Handbook*, edited by W. S. Levine, CRC Press, Boca Raton, FL, 1996, pp. 941–951.

[17]DeCarlo, R. A., Zak, S. H., and Mathews, G. P., "Variable Structure Control of Nonlinear Multivariable Systems: A Tutorial," *Proceedings of the IEEE*, Vol. 76, No. 3, 1988, pp. 212–232.

[18]Fernández, B. R., and Hedrick, J. K., "Control of Multivariable Non-Linear Systems by the Sliding Mode Method," *International Journal of Control*, Vol. 46, No. 3, 1987, pp. 1019–1040.

[19]Hung, J. Y., Weibing, G., and Hung, J. C., "Variable Structure Control: A Survey," *IEEE Transactions on Industrial Electronics*, Vol. 40, No. 1, 1993, pp. 2–23.

[20]Utkin, V. I., "Sliding Mode Control Design Principles and Applications to Electric Drives," *IEEE Transactions on Industrial Electronics*, Vol. 40, No. 1, 1993, pp. 23–36.

[21]Edwards, C., and Spurgeon, S. K., *Sliding Mode Control*, Taylor and Francis, Bristol, PA, 1998, Chap. 3.

[22]Shtessel, Y. B., Buffington, J. M., and Banda, S. S., "Multiple Timescale Flight Control Using Reconfigurable Sliding Modes," *Journal of Guidance, Control, and Dynamics*, Vol. 22, No. 6, 1999, pp. 873–883.

[23]Shtessel, Y. B., Buffington, J. M., and Banda, S. S., "Tailless Aircraft Flight Control Using Multiple Time Scale Reconfigurable Sliding Modes," AIAA Paper 99-4136, Aug. 1999.

[24]Shtessel, Y. B., Buffington, J. M., Pachter, M., Chandler, P. R., and Banda, S. S., "Reconfigurable Flight Control on Sliding Modes Addressing Actuator Deflection and Deflection Rate Saturation," AIAA Paper 98-4112, Aug. 1998.

[25]Slotine, J.-J. E., and Li, W., *Applied Nonlinear Control*, Prentice–Hall, Englewood Cliffs, NJ, 1991, Chap. 6.

[26]Johnson, E. N., Calise, A. J., El-Shirbiny, H. A., and Rysdyk, R. T., "Feedback Linearization with Neural Network Augmentation Applied to X-33 Attitude Control," AIAA Paper 2000-4157, Aug. 2000.

[27]Hess, R. A., "Unified Theory for Aircraft Handling Qualities and Adverse Aircraft–Pilot Coupling," *Journal of Guidance, Control, and Dynamics*, Vol. 20, No. 6, 1997, pp. 1141–1148.

[28]Siwakosit, W., Snell, S. A., and Hess, R. A., "Robust Flight Control Design with Handling Qualities Constraints Using Scheduled Linear Dynamic Inversion and Loop-Shaping," *IEEE Transactions on Control Systems Technology*, Vol. 8, No. 3, 2000, pp. 483–494.

[29]Maciejowski, J. M., *Multivariable Feedback Design*, Addison Wesley Longman, Wokinghman, England, U.K., 1989, Chap. 1.

[30]"Innovative Control Effectors," U.S. Air Force Research Lab., WL-TR-96-3043, Wright–Patterson AFB, OH, Jan. 1996.

[31]Bacon, B. J., and Ostroff, A. J., "Reconfigurable Flight Control Using Nonlinear Dynamic Inversion with a Special Accelerometer Implementation," AIAA Paper 2000-4565, Aug. 2000.

[32]Barker, J. M., and Balas, G. J., "Flight Control of a Tailless Aircraft Via Linear Parameter-Varying Techniques," AIAA Paper 99-4133, Aug. 1999.

[33]Buffington, J. M., "Tailless Aircraft Control Allocation," AIAA Paper 97-3605, 1997.

[34]Buffington, J. M., Chandler, P. R., and Pachter, M., "Integration of On-Line System Identification and Optimization-Based Control Allocation," AIAA Paper 98-4487, Aug. 1998.

[35]Buffington, J. M., and Shtessel, Y. B., "Saturation Protection for Feedback Linearizable Systems Using Sliding Mode Theory," *Proceedings of American Control Conference*, Vol. 2, IEEE Publications, Piscataway, NJ, 1998, pp. 1028–1032.

[36]Buffington, J. M., Chandler, P. R., and Pachter, M., "On-Line System Identification for Aircraft with Distributed Control Effectors," *International Journal of Robust and Nonlinear Control*, Vol. 9, 1999, pp. 1033–1049.

[37]Page, A. B., and Steinberg, M. L., "A Closed-Loop Comparison on Control Allocation Methods," AIAA Paper 2000-4538, Aug. 2000.

[38]Hess, R. A., Zeyada, Y., and Heffley, R. K., "Modeling and Simulation for Helicopter Task Analysis," *Journal of the American Helicopter Society*, Vol. 47, No. 4, 2002, pp. 243–252.